

Fast Machine-Precision Spectral Likelihoods for Stationary Time Series

Christopher J. Geoga ^{*†}

Abstract

We provide in this work an algorithm for approximating a very broad class of symmetric Toeplitz matrices to machine precision in $\mathcal{O}(n \log n)$ time with applications to fitting time series models. In particular, for a symmetric Toeplitz matrix Σ with values $\Sigma_{j,k} = h_{|j-k|} = \int_{-1/2}^{1/2} e^{2\pi i|j-k|\omega} S(\omega) d\omega$ where $S(\omega)$ is piecewise smooth, we give an approximation $\mathcal{F}\Sigma\mathcal{F}^H \approx \mathbf{D} + \mathbf{U}\mathbf{V}^H$, where \mathcal{F} is the DFT matrix, \mathbf{D} is diagonal, and the matrices \mathbf{U} and \mathbf{V} are in $\mathbb{C}^{n \times r}$ with $r \ll n$. Studying these matrices in the context of time series, we offer a theoretical explanation of this structure and connect it to existing spectral-domain approximation frameworks. We then give a complete discussion of the numerical method for assembling the approximation and demonstrate its efficiency for improving Whittle-type likelihood approximations, including dramatic examples where a correction of rank $r = 2$ to the standard Whittle approximation increases the accuracy from 3 to 14 digits for a matrix $\Sigma \in \mathbb{R}^{10^5 \times 10^5}$. The method and analysis of this work applies well beyond time series analysis, providing an algorithm for extremely accurate direct solves with a wide variety of symmetric Toeplitz matrices. The analysis employed here largely depends on asymptotic expansions of oscillatory integrals, and also provides a new perspective on when existing spectral-domain approximation methods for Gaussian log-likelihoods can be particularly problematic.

1 Introduction

A mean-zero, stationary, and Gaussian time series is a stochastic process $\{Y_t\}_{t \in \mathbb{Z}}$ such that any contiguous collection of measurements $\mathbf{y} = [Y_{t_0}, Y_{t_0+1}, \dots, Y_{t_0+n-1}]$ with arbitrary $t_0 \in \mathbb{Z}$ is distributed as $\mathbf{y} \sim \mathcal{N}(\mathbf{0}, \Sigma)$, where $\Sigma_{j,k} = h_{|j-k|}$ is the autocovariance matrix generated by the autocovariance sequence $\{h_k\}_{k \in \mathbb{Z}}$. A very special property of such covariance matrices for stationary time series is that they are symmetric *Toeplitz* matrices, meaning that they are constant along sub- and super-diagonal bands. A fundamental and important problem in time series analysis is fitting a parametric model to data, which in this setting means using some parametric family of models for the autocovariance sequence $\{h_k(\boldsymbol{\theta})\}_{k \in \mathbb{Z}}$ that specify the distribution $\mathbf{y} \sim \mathcal{N}(\mathbf{0}, \Sigma(\boldsymbol{\theta}))$ (like, for example, (AR)(I)(MA) process models). The canonical estimator for parameters $\boldsymbol{\theta} \in \Theta$ from data is the maximum likelihood estimator (MLE), which is computed by minimizing the negative log-likelihood:

$$\hat{\boldsymbol{\theta}}^{\text{MLE}} = \arg \min_{\boldsymbol{\theta} \in \Theta} \ell(\boldsymbol{\theta} | \mathbf{y}) = \arg \min_{\boldsymbol{\theta} \in \Theta} \frac{1}{2} (\log |\Sigma(\boldsymbol{\theta})| + \mathbf{y}^T \Sigma(\boldsymbol{\theta}) \mathbf{y}),$$

where constant terms in the negative log-likelihood $\ell(\boldsymbol{\theta} | \mathbf{y})$ are suppressed.

It is an elementary fact that autocovariance sequences are positive (semi-)definite, and by Herglotz's theorem one has that

$$h_k = \int_{[-1/2, 1/2)} e^{2\pi i k \omega} dF(\omega),$$

where F is the *spectral distribution function* [9]. If F has a density with respect to the Lebesgue measure so that $dF(\omega) = S(\omega) d\omega$, we call $S(\omega)$ the *spectral density function* (SDF). An elementary property of spectral densities is that they need only be non-negative, and symmetric about the origin in the case of real-valued processes Y_t . Considering that writing parametric families of functions that are nonnegative and symmetric

^{*}Dept. of Statistics, University of Wisconsin-Madison

[†]geoga@wisc.edu

is much easier than writing parametric families of sequences that are positive (semi-)definite, it comes as no surprise that modeling $\{h_k(\boldsymbol{\theta})\}_{k \in \mathbb{Z}}$ in terms of the spectral density $S_{\boldsymbol{\theta}}(\omega)$ is an attractive and liberating option for practitioners.

Unfortunately, there is no particularly easy way to reformulate $\ell(\boldsymbol{\theta} | \mathbf{y})$ directly in terms of $S(\omega)$, meaning that computing the true MLE $\hat{\boldsymbol{\theta}}^{\text{MLE}}$ requires either knowing the closed-form expression for $h_k = \int_{-1/2}^{1/2} e^{2\pi i \omega k} S(\omega) d\omega$ for all k or directly computing all the integrals numerically. As we will discuss, there are several popular likelihood approximations for \mathbf{y} in terms of $S_{\boldsymbol{\theta}}(\omega)$ that are convenient and computationally expedient, often running in $\mathcal{O}(n \log n)$ complexity compared to the $\mathcal{O}(n^3)$ of a direct likelihood approximation (another fundamental challenge that motivates many spectral approximations). The most classical and simple of these approximations to $\ell(\boldsymbol{\theta} | \mathbf{y})$, denoted the *Whittle approximation* [32], unfortunately yields very biased estimators. Improvements to this method can mitigate the challenging new sources of bias, but still come at the cost of additional variability compared to $\hat{\boldsymbol{\theta}}^{\text{MLE}}$. In this work, we introduce a new approximation to $\ell(\boldsymbol{\theta} | \mathbf{y})$ that retains the $\mathcal{O}(n \log n)$ complexity but can be made effectively exact to double precision with 14 – 15 correct digits by exploiting piecewise smoothness of spectral densities and special rank structure in the matrix $\mathcal{F}\boldsymbol{\Sigma}\mathcal{F}^H$, where \mathcal{F} is the discrete Fourier transform (DFT) matrix. As a result of this design, we obtain effectively exact evaluations of the log-likelihood $\ell(\boldsymbol{\theta} | \mathbf{y})$ and its derivatives and the ability to perform uncertainty quantification on estimates.

1.1 Whittle approximations and existing work

Let $J_n(\omega) = \frac{1}{\sqrt{n}} \sum_{j=0}^{n-1} e^{-2\pi i j \omega} Y_j$ denote the discrete Fourier transform of a time series $\{Y_0, \dots, Y_{n-1}\}$ at frequency ω . For the entirety of this work, we will restrict focus to ω at Fourier frequencies $\left\{ \omega_j = \frac{(j-n/2-1)}{n} \right\}_{j=1}^n$ so that one can compute $[J_n(\omega_1), \dots, J_n(\omega_n)]$ in $\mathcal{O}(n \log n)$ time with $\mathcal{F}\mathbf{y}$ using an FFT, where \mathcal{F} is parameterized in the unitary form with the “fftshift” for convenience as $\mathcal{F} = [n^{-1/2} e^{-2\pi i j k / n}]_{j \in (-n/2):(n/2-1), k \in 0:(n-1)}$. Motivated by the elementary observations that $\mathbb{E}|J_n(\omega_k)|^2 \rightarrow_n S(\omega_k)$ and $\text{Cov}(J_n(\omega_k), J_n(\omega_{k'})) \rightarrow_n 0$ (see [9] for an introduction), the Whittle approximation $\ell^W(\boldsymbol{\theta} | \mathbf{y}) \approx \ell(\boldsymbol{\theta} | \mathbf{y})$ is defined as

$$2\ell^W(\boldsymbol{\theta} | \mathbf{y}) = \sum_{j=1}^n \log S_{\boldsymbol{\theta}}(\omega_j) + \frac{|J_n(\omega_j)|^2}{S_{\boldsymbol{\theta}}(\omega_j)}. \quad (1.1)$$

Optimizing this approximation instead of $\ell(\boldsymbol{\theta} | \mathbf{y})$ gives the estimator $\hat{\boldsymbol{\theta}}^W$. Another way to think about this approximation is by observing that it effectively approximates $\boldsymbol{\Sigma}(\boldsymbol{\theta})$ with the *circulant* matrix \mathbf{C} whose first column \mathbf{c} has $(\mathcal{F}\mathbf{c})_j = S(\omega_j)$. This is unfortunately incorrect in the sense that $\boldsymbol{\Sigma}$ is almost never exactly circulant—and even if it were, it wouldn’t in general for any finite n be *that* circulant matrix. As a result of these finite-sample applications of limiting identities, this estimator can exhibit severe bias for finite sample sizes and certain varieties of spectral densities $S(\omega)$ —see [28] for a particularly thoughtful and concrete analysis of the sources of bias of this approximation in terms of boundary effects. Another way to understand the source of bias with this approximation is to observe that even if $\mathbf{y} \sim \mathcal{N}(\mathbf{0}, \boldsymbol{\Sigma}(\boldsymbol{\theta}_0))$ with $\boldsymbol{\Sigma}(\boldsymbol{\theta}_0)_{j,k} = \int_{-1/2}^{1/2} e^{2\pi i \omega |j-k|} S_{\boldsymbol{\theta}_0}(\omega) d\omega$, $S_{\boldsymbol{\theta}_0}(\omega_k)$ is *not* the variance of $J_n(\omega_k)$ for any finite n . And while ignoring covariance structure between values (which this approximation also does) can in some cases only come at the cost of efficiency, using incorrect variances will almost always come at the cost of bias. The exact (co)variances of these DFT coefficients is a classical computation, but because they will be used extensively in this work we provide a terse statement of their derivation here. As we will see in greater detail in subsequent sections, even for very large n the difference between $S(\omega_k)$ and the finite-sample variance of $J_n(\omega_k)$ can be substantial.

Proposition 1. *Let $\{Y_t\}_{t=0}^{n-1}$ be a stationary mean-zero time series with spectral density $S(\omega)$ and $J_n(\omega_k)$ defined as above, and define $S_n(\omega_k, \omega_{k'}) = \text{Cov}(J_n(\omega_k), J_n(\omega_{k'}))$. Then*

$$S_n(\omega_k, \omega_{k'}) = \frac{e^{i \frac{n-1}{n} \pi (k-k')}}{n} \int_{-1/2}^{1/2} D_n^s(\omega_k - \omega) D_n^s(\omega_{k'} - \omega) S(\omega) d\omega, \quad (1.2)$$

where $D_n^s(\omega) = \frac{\sin(\pi n \omega)}{\sin(\pi \omega)} = e^{-i(n-1)\omega/2} \sum_{j=0}^{n-1} e^{2\pi i j \omega}$ is a “shifted” Dirichlet kernel.

Proof. Using Herglotz’s theorem above, an elementary computation shows that

$$\begin{aligned} \text{Cov}(J_n(\omega_k), J_n(\omega_{k'})) &= \int_{-1/2}^{1/2} \left(\sum_{j=0}^{n-1} n^{-1/2} e^{2\pi i j(\omega - \omega_k)} \right) \left(\sum_{j=0}^{n-1} n^{-1/2} e^{2\pi i j(\omega_{k'} - \omega)} \right) S(\omega) d\omega \\ &= \frac{1}{n} \int_{-1/2}^{1/2} \left(e^{-i(n-1)\pi\omega_k} \frac{\sin(\pi n(\omega_k - \omega))}{\sin(\pi(\omega_k - \omega))} \right) \left(e^{i(n-1)\pi\omega_{k'}} \frac{\sin(\pi n(\omega_{k'} - \omega))}{\sin(\pi(\omega_{k'} - \omega))} \right) S(\omega) d\omega, \end{aligned}$$

Applying the definition of $D_n^s(\omega)$, collecting terms, and bringing the complex exponential prefactor on the sin terms outside the integral gives the results. \square

A particularly elegant proposition for dealing with the bias of $\hat{\theta}^W$ is given in [29]: instead of using $S_{\theta}(\omega_j)$ in ℓ^W , directly use $S_n(\omega_j, \omega_j)$ in its place. By providing the correct finite-sample variances for the DFT coefficients, one immediately obtains a new likelihood approximation whose gradient gives unbiased estimating equations for parameters θ [29, 22]. This estimator, called the *debiased* Whittle estimator, is given as

$$\hat{\theta}^{DW} = \arg \min_{\theta \in \Theta} \ell^{DW}(\theta | \mathbf{y}) = \arg \min_{\theta \in \Theta} \frac{1}{2} \left(\sum_{j=1}^n \log S_{n,\theta}(\omega_j, \omega_j) + \frac{|J_n(\omega_j)|^2}{S_{n,\theta}(\omega_j, \omega_j)} \right),$$

and now only comes at the cost of additional variance from ignoring the correlation of $J_n(\omega_k)$ with $J_n(\omega_{k'})$. This method will serve as a useful point of comparison with the one proposed here in the sense that it better isolates the additional variance of Whittle-type estimators compared to $\hat{\theta}^{\text{MLE}}$.

While the standard Whittle approximation requires pre-computed FFT of the data, this approximation requires one FFT per evaluation of $\ell^{DW}(\theta | \mathbf{y})$, since one can compute $\{S_n(\omega_j, \omega_j)\}_{j=1}^n$ in the time domain using the classical identity that

$$S_n(\omega_j, \omega_j) = 2\text{Re} \left\{ \sum_{k=0}^{n-1} (1 - n^{-1}h) h_k e^{-2\pi i \omega_j h} \right\} - h_0. \quad (1.3)$$

In [29] it is noted that this identity is useful to avoid numerical integration. While this is true, it is also quite *inconvenient* in that it requires knowing the covariance function as well as the spectral density. Considering that a large part of the point of resorting to a Whittle-type approximation is to write a parametric spectral density instead of a covariance. In the next section, in the process of building up to our own approximation, we will discuss two performant and simple numerical integration strategies to relax this requirement and also makes this method more generally available to practitioners.

1.2 Our method

The approximation we introduce here is a continuation of such spectrally motivated likelihood methods. Letting Σ denote the Toeplitz covariance matrix for a time series with spectral density $S(\omega)$ and \mathbf{D} denote the diagonal matrix with values $\{S(\omega_j)\}_{j=1}^n$, the fundamental observation of this work is that for a very broad class of spectral densities we have that

$$\mathcal{F}\Sigma\mathcal{F}^H \approx \mathbf{D} + \mathbf{U}\mathbf{V}^H, \quad (1.4)$$

where \mathbf{U} and \mathbf{V} are in $\mathbb{C}^{n \times r}$ with $r \ll n$. The standard Whittle approximation views that low-rank update as being exactly zero, and in this light our method can be viewed as a “corrected” Whittle approximation. The key observation that makes working with this approximation convenient is that the “Whittle correction” matrix $\mathbf{C} = \mathcal{F}\Sigma\mathcal{F}^H - \mathbf{D}$, along with being severely rank-deficient in many settings, can be applied to a vector in $\mathcal{O}(n \log n)$ complexity via circulant embedding of Toeplitz matrices, and so one can utilize the very powerful methods of randomized low-rank approximation [21] to assemble \mathbf{U} and \mathbf{V} efficiently and scalably with implicit tools.

Despite having the same quasilinear runtime complexity, for very small r (sometimes as small as $r = 2$), this representation can be *exact* to computer precision. As one might expect, this does come at the cost of a

more expensive prefactor. If the standard Whittle approximation requires one pre-computed FFT of the data and subsequently runs at linear complexity, and the debiased Whittle approximation requires one additional FFT per evaluation due to computation of the terms in (1.3), our approximation requires $\mathcal{O}(3r)$ FFTs to assemble (although a simpler implementation using $\mathcal{O}(4r)$ FFTs is used in the computations of this work¹). For a spectral density that is neither particularly well- nor poorly-behaved, a reasonable expectation for an r that gives all 14 significant digits of $\ell(\boldsymbol{\theta} | \mathbf{y})$ is around $r \approx 100$ —and so for full precision of the likelihood, this method can require several hundred FFTs. This is an undeniably more expensive likelihood approximation, and there will of course be circumstances in which a practitioner may choose a cheaper option at the cost of efficiency or bias. But considering how fast FFTs are, the prefactor cost for this method is sufficiently low that it compares favorably with other high-accuracy alternatives.

Another material advantage of this method over other spectral approximations is that it can be used to compute uncertainties for estimators. A basic fact about MLEs is that, under sufficient regularity conditions, $\mathbf{I}(\boldsymbol{\theta})^{-1/2}(\hat{\boldsymbol{\theta}}^{\text{MLE}} - \boldsymbol{\theta}^{\text{true}}) \rightsquigarrow \mathcal{N}(\mathbf{0}, \boldsymbol{\mathcal{I}})$, where $\mathbf{I}(\boldsymbol{\theta})$ is the expected Fisher information matrix that will be introduced and discussed at length later in this work, although in some settings it may actually be preferable to use the “observed” information matrix $H\ell(\boldsymbol{\theta} | \mathbf{y})|_{\boldsymbol{\theta}=\hat{\boldsymbol{\theta}}^{\text{MLE}}}$ [13]. This latter observation highlights an issue: even if some approximation $\tilde{\ell}(\boldsymbol{\theta} | \mathbf{y}) \approx \ell(\boldsymbol{\theta} | \mathbf{y})$ has a minimizer *exactly* at $\hat{\boldsymbol{\theta}}^{\text{MLE}}$, that certainly does not mean that their Hessians at $\hat{\boldsymbol{\theta}}^{\text{MLE}}$ are equal or even similar. This is why, in general, one cannot directly use derivative information of an approximated log-likelihood to perform inferential tasks about estimated parameters. Considering that our approximation to the likelihood is effectively exact to double precision, however, it *can* be used for uncertainty quantification of estimates $\hat{\boldsymbol{\theta}}$. More generally, unlike very technical hierarchical matrix approximations that are often used to approximate covariance matrices [2, 14, 25, 24, 15], this very simple representation means that it is trivial to compute several quantities beyond just the log-likelihood that are useful for estimation or uncertainty quantification. One example quantity is the exact gradient of the log-likelihood, which requires matrix-matrix products. Matrix-matrix products are often a challenge that hierarchical matrix-based methods have to circumvent in this context by using stochastic trace approximations [3, 27, 15] or peeling [25], which result in stochastic gradients that can make using high-quality optimization libraries difficult. It is also trivial to implement symmetric factorizations, fully compute and instantiate inverses, and many other operations that are often unavailable or problematically expensive to do with more sophisticated matrix compression structures.

1.3 Outline

In the next several sections, we will introduce tools for implicitly assembling and working with matrices of the form (1.4). We start with a discussion of using quadrature and asymptotic expansions to efficiently and accurately work with $\boldsymbol{\Sigma}$ using only the spectral density $S(\omega)$, and we then provide a discussion of (i) why the perturbation term in (1.4) should be low-rank, which also offers a new theoretical perspective for when Whittle approximations are particularly problematic, and (ii) the details of assembling the low-rank UV^H entirely from fast matrix-vector products. We then close by providing several tests and benchmarks to demonstrate the speed and accuracy of the method.

2 Oscillatory integration of spectral densities

As discussed in the previous section, creating the low-rank approximation $\mathcal{F}\boldsymbol{\Sigma}\mathcal{F}^H \approx \mathbf{D} + UV^H$ requires working with $\boldsymbol{\Sigma}$, the Toeplitz matrix with values $\Sigma_{j,k} = h_{|j-k|}$ where $\{h_k\}$ is the autocovariance sequence of the time series. Unlike in [29] where both kernel and spectral density values are used to avoid numerical integration, we will now discuss strategies for efficiently and accurately computing integrals of the form

$$h_k = \int_{-1/2}^{1/2} S(\omega) e^{2\pi i k \omega} d\omega \quad (2.1)$$

for $k \in 0, \dots, n$ so that one can create this factorization given only the spectral density. Let us briefly review the challenges of such a task. First, the standard method for obtaining the values $\{h_k\}$ using the trapezoidal

¹A software package and scripts for all computations done in this work is available at <https://github.com/cgeoga/SpectralEstimators.jl>.

rule via the FFT may require a large number of nodes for even moderate accuracy if, for example, $S(\omega)$ has rough points (like how $S(\omega) = e^{-|\omega|}$ has no derivatives at the origin). A second common issue arises if $S(\omega)$ is not periodic at its endpoints, which limits the convergence rate of the trapezoidal rule to its baseline rate of $\mathcal{O}(m^{-2})$ for m nodes for general non-smooth and/or non-periodic integrands. Even if one instead opts to use a higher-order quadrature rule like Gauss-Legendre, for example, the Shannon-Nyquist sampling theorem still requires at least $\mathcal{O}(k)$ many nodes to resolve the oscillations of $e^{2\pi i k \omega}$. The difficulty that this poses is that if you need to evaluate h_k out to, say, $k = 10\,000$, those last values in the sequence will pose a significant computational burden.

To bypass these issues, we propose the use of adaptive Gauss-Legendre quadrature for a fixed number of lags k , but then a transition to the use of asymptotic expansions to h_k for lags greater than some k_0 . For integrands that are not too oscillatory, say for $k \leq 2\,000$ (the cutoff used in all computations of this work), standard adaptive integration tools can be very efficient and capable for any piecewise-smooth integrand. In this work, the Julia language package `QuadGK.jl` [7, 23] was used, although many other tools would likely have worked equally well. Briefly, Gaussian quadrature is a tool for achieving high-order accuracy in the numerical integration of smooth functions. It gives approximations to integrals as

$$\int_a^b f(x) dx \approx \sum_{j=1}^M \alpha_j f(x_j)$$

that are exact for polynomials up to order $2M - 1$, where $\{\alpha_j\}_{j=1}^M$ are *weights* and $\{x_j\}_{j=1}^M$ are *nodes*. In the case of $[a, b] = [-1, 1]$ the Legendre polynomials can be used to obtain the weights and nodes and achieve an error rate of $\mathcal{O}(M^{-2m-1})$ for functions $f \in \mathcal{C}^{(m)}([a, b])$ [30]. These integrals can easily be made adaptive by computing their discretized approximation for orders $2M - 1$ and $3M + 1$, as is done in Gauss-Kronrod quadrature, for example, and concluding that the approximation has converged when these quantities agree to a prescribed tolerance [16].

More interesting, however, is the discussion of methods for accurately and efficiently computing h_k when k is large. Unlike traditional integration tools, asymptotic expansion-type methods get *more* accurate as k increases. As in the introduction, the following result is not new (see [11] for a comprehensive discussion), but we state it in the specific form that is useful for this work since it will be referred to frequently. Since the idea of the proof is also used repeatedly, we again provide a terse proof.

Proposition 2. *Let $S(\omega) \in \mathcal{C}^{(m)}([-1/2, 1/2])$ and $\int_{-1/2}^{1/2} |S^{(m)}|(\omega) d\omega < C < \infty$. Then*

$$\int_{-1/2}^{1/2} S(\omega) e^{2\pi i k \omega} d\omega = - \sum_{j=0}^{m-1} (-i2\pi k)^{-(j+1)} (S^{(j)}(1/2) e^{\pi i k} - S^{(j)}(-1/2) e^{-\pi i k}) + \mathcal{O}(k^{-m-1}).$$

Proof. Simply apply integration by parts as many times as possible:

$$\begin{aligned} \int_{-1/2}^{1/2} S(\omega) e^{2\pi i k \omega} d\omega &= \frac{S(1/2) e^{\pi i k} - S(-1/2) e^{-\pi i k}}{-2\pi i k} + (-2\pi i k)^{-1} \int_{-1/2}^{1/2} S'(\omega) e^{2\pi i k \omega} d\omega \\ &\vdots \\ &= \sum_{j=0}^{m-1} (-2\pi i k)^{-(j+1)} (S^{(j)}(1/2) e^{\pi i k} - S^{(j)}(-1/2) e^{-\pi i k}) \\ &\quad + (-2\pi i k)^{-(m+1)} \int_{-1/2}^{1/2} S^{(m)}(\omega) e^{2\pi i k \omega} d\omega. \end{aligned}$$

□

Remarkably, evaluating this expansion for *any* lag k only requires a few derivatives of $S(\omega)$ at its endpoints. For this reason, with this tool evaluating the tail of $\{h_k\}$ for high frequencies k actually becomes the fastest part of the domain to handle. And while the supposition of the above theorem that $S \in \mathcal{C}^m([-1/2, 1/2])$ is obviously restrictive, a simple observation extends this result to a much broader class of functions.

Corollary 1. Let $S(\omega) \in \mathcal{C}^{(m)}([-1/2, 1/2] \setminus \{\omega_1^r, \dots, \omega_L^r\})$, so that it is smooth except at locations $\{\omega_1^r, \dots, \omega_L^r\}$, further assume that at each ω_l^r it has at least m directional derivatives $S^{(m\pm)}(\omega_l^r)$ from both the left ($m-$) and the right ($m+$) for $l \in 1, \dots, L$. Then

$$\int_{-1/2}^{1/2} S(\omega) e^{2\pi i k \omega} d\omega = \sum_{l=1}^{L-1} \sum_{j=0}^{m-1} (-2\pi i k)^{-(j+1)} (S^{(j-)}(\omega_{l+1}^r) e^{2\pi i k \omega_{l+1}^r} - S^{(j+)}(\omega_l^r) e^{2\pi i k \omega_l^r}) + \mathcal{O}(k^{-m-1}).$$

This corollary, which is proven by simply breaking up the domain $[-1/2, 1/2]$ into segments with endpoints at each ω_l^r and applying the above argument to each segment, now means that this asymptotic expansion approach can be used to accurately calculate h_k for very large k for any spectral density that is just *piecewise* smooth. The prefactor on the error term in this setting is naturally increased compared to the setting of Proposition 2. Nonetheless, however, the convergence rates are on our side. For example, if $k = 3000$ and one uses five derivatives, then the error term in the simple case is given by $C \cdot (6,000\pi)^{-6} \approx C \cdot 10^{-26}$. For a spectral density like $S(\omega) = 10e^{-10|\omega|}$, an example that will be studied extensively in later sections due to being well-behaved except at the origin, we see that $h_{3000} \approx 5 \cdot 10^{-7}$. For that particular function, then, this bound indicates that unless C is quite large one can reasonably expect a full 14 – 15 digits of accuracy. Considering that this evaluation method uses only derivatives of $S(\omega)$ at the endpoint and takes just a few nanoseconds on a modern CPU once those have been pre-computed, this combination of adaptive Gauss-Legendre quadrature for sufficiently low lags k and asymptotic expansions for the rest gives $\{h_k\}_{k=0}^{n-1}$ for all lags quickly and accurately.

An alternative way to compute $\{h_k\}_{k=1}^n$ for potentially large n in $\mathcal{O}(n \log n)$ time is to use nonuniform fast Fourier transforms (NUFFT) and Gauss-Legendre quadrature to evaluate h_k at *all* lags [12, 5]. While the traditional FFT algorithm critically depends on measurements being given on a regular grid and exploits the symmetries that that creates, NUFFTs are fast algorithms to evaluate sums of complex exponentials at potentially irregular locations and target frequencies in quasilinear runtime. Per the discussion above, we see that computing $\{h_k\}_{k=1}^n$ would require $M = \mathcal{O}(n)$ quadrature nodes (to resolve the highest frequencies) and naturally needs to be evaluated at n target values, which means that naive computation of those integrals would require $\mathcal{O}(n^2)$ work. With the NUFFT, however, the sums can be computed as a matrix-vector product

$$\begin{bmatrix} h_0 \\ n_1 \\ \vdots \\ h_{n-1} \end{bmatrix} = \begin{bmatrix} \alpha_1 e^{2\pi i \omega_1^q 0} & \alpha_2 e^{2\pi i \omega_2^q 0} & \dots & \alpha_M e^{2\pi i \omega_M^q 0} \\ \alpha_1 e^{2\pi i \omega_1^q 1} & \alpha_2 e^{2\pi i \omega_2^q 1} & \dots & \alpha_M e^{2\pi i \omega_M^q 1} \\ \vdots & \vdots & \ddots & \vdots \\ \alpha_1 e^{2\pi i \omega_1^q (n-1)} & \alpha_2 e^{2\pi i \omega_2^q (n-1)} & \dots & \alpha_M e^{2\pi i \omega_M^q (n-1)} \end{bmatrix} \begin{bmatrix} S(\omega_1^q) \\ S(\omega_2^q) \\ \vdots \\ S(\omega_M^q) \end{bmatrix}$$

in $\mathcal{O}(n \log n)$ time, where ω_k^q denotes the k -th quadrature weight. This method, while much more expensive than using asymptotic expansions, has the advantage that it does not require computing any derivatives to evaluate the sequence $\{h_k\}_{k=1}^n$. Because of this, it can be more accurate for SDFs $S(\omega)$ with higher-order derivatives that potentially get very large or are for some other reason numerically unstable to compute. With that said, however, as discussed above the accuracy of Gauss-Legendre quadrature depends heavily on how smooth the integrand is. So we still recommend splitting the domain $[-1/2, 1/2]$ into panels such that the rough points of $S(\omega)$ are endpoints, just as with the splitting of the asymptotic expansions. For a much more detailed discussion of numerical Fourier integration of spectral densities and the quadrature-based tools introduced here for doing it quickly, we refer readers to [6].

3 Low rank structure of the Whittle correction

We now turn to the question of *why* one should expect the matrix

$$C = \mathcal{F} \Sigma \mathcal{F}^H - D,$$

where D is diagonal with $D_{j,j} = S(\omega_j)$, to be of low numerical rank. The primary tool for this investigation will again be asymptotic expansions, and perhaps the crucial observation is that for every k and k' , $C_{k,k'}$ is given by an oscillatory integral with the same high frequency of $2\pi n$. While the below analysis is not actually

how we choose to compute and assemble this low-rank approximation in this work, the following derivation provides some idea for why the Whittle correction matrix \mathbf{C} has low-rank structure, even when S is not smooth or $\{h_k\}$ decays slowly. For the duration of this section, we will assume that $S(\omega) \in \mathcal{C}^{(m)}([-1/2, 1/2])$ for convenience, although the results here can again be extended using directional derivatives if S is not differentiable but is smooth from the left and the right at rough points.

We begin by adding and subtracting $S(\omega_k)$ and $S(\omega_{k'})$ to the inner integrand in (1.2), which with minor simplification steps can be expressed as

$$\begin{aligned} & \frac{1}{n} \int_{-1/2}^{1/2} D_n^s(\omega_k - \omega) D_n^s(\omega_{k'} - \omega) S(\omega) d\omega \\ &= \frac{1}{2n} \int_{-1/2}^{1/2} D_n^s(\omega_k - \omega) D_n^s(\omega_{k'} - \omega) (S(\omega) - S(\omega_k)) d\omega \\ & \quad + \frac{1}{2n} \int_{-1/2}^{1/2} D_n^s(\omega_k - \omega) D_n^s(\omega_{k'} - \omega) (S(\omega) - S(\omega_{k'})) d\omega \\ & \quad + \frac{S(\omega_k) + S(\omega_{k'})}{2n} \int_{-1/2}^{1/2} D_n^s(\omega_k - \omega) D_n^s(\omega_{k'} - \omega) d\omega. \end{aligned} \quad (3.1)$$

While unwieldy, this representation of the integral already provides a reasonably direct explanation about several features of $\mathcal{F}\Sigma\mathcal{F}^H$. Recalling that

$$\int_{-1/2}^{1/2} D_n^s(\omega_k - \omega) D_n^s(\omega_{k'} - \omega) d\omega = \begin{cases} n & k = k' \\ 0 & k \neq k' \end{cases},$$

we see that the third term is precisely the diagonal contribution of $S(\omega_k)$. Now we will now argue that the first two terms in the above sum correspond to severely rank-deficient matrices. Since they can of course be analyzed in the exact same way, we study only the first in detail here.

To begin, we slightly rewrite the first term in (3.1) as

$$\int_{-1/2}^{1/2} \sin(\pi n(\omega_k - \omega)) \sin(\pi n(\omega_{k'} - \omega)) \csc(\pi(\omega_k - \omega)) \csc(\pi(\omega_{k'} - \omega)) (S(\omega) - S(\omega_k)) d\omega. \quad (3.2)$$

From here, we partition the domain into

$$[-1/2, 1/2] = \underbrace{[-1/2, \omega_k - \gamma]}_{\text{Type I}} \cup \underbrace{B_\gamma(\omega_k)}_{\text{Type II}} \cup \underbrace{[\omega_k + \gamma, \omega_{k'} - \gamma]}_{\text{Type I}} \cup \underbrace{B_\gamma(\omega_{k'})}_{\text{Type II}} \cup \underbrace{[\omega_{k'} + \gamma, 1/2]}_{\text{Type I}}, \quad (3.3)$$

where $B_\gamma(x) = [x - \gamma, x + \gamma]$ and γ is some small number chosen to keep distance from the singularities of the cosecant terms—for example, a value of $\gamma = 0.001$. By design, then, in Type I intervals the cosecant terms are simple analytic functions. Defining

$$\tilde{S}_{n,k,k'}(\omega) = \csc(\pi(\omega_k - \omega)) \csc(\pi(\omega_{k'} - \omega)) (S(\omega) - S(\omega_k)), \quad (3.4)$$

we see that in Type I regions this function is bounded above (assuming that S itself is) and as smooth as S . This motivates the following result that will be used many times in this section.

Proposition 3. *If $g(\omega) \in \mathcal{C}^{(m)}([a, b])$ and $g^{(m)}$ is integrable on $[a, b]$, then*

$$\begin{aligned} \int_a^b \sin(\pi n(\omega_k - \omega)) \sin(\pi n(\omega_{k'} - \omega)) g(\omega) d\omega &= \frac{1}{2} \left[\int_a^b g(\omega) d\omega \right] (-1)^{k-k'} \\ & \quad - \frac{1}{2} \Re \left\{ e^{i\pi n \frac{k+k'}{2}} \left[e^{2\pi i b} \sum_{j=0}^{m-1} \frac{g^{(j)}(b)}{(-i2\pi n)^{j+1}} - e^{2\pi i a} \sum_{j=0}^{m-1} \frac{g^{(j)}(a)}{(-i2\pi n)^{j+1}} \right] \right\} \\ & \quad + \mathcal{O}(n^{-m-1}). \end{aligned} \quad (3.5)$$

Proof. Using the product-to-sum angle formula that $\sin(\theta)\sin(\phi) = \frac{1}{2}(\cos(\theta - \phi) - \cos(\theta + \phi))$ and standard manipulations of the complex exponential, the left hand side equation can be re-written as

$$\frac{1}{2} \cos\left(\pi n \frac{k - k'}{n}\right) \int_a^b g(\omega) d\omega + \frac{1}{2} \Re \left\{ e^{i\pi n \frac{k+k'}{2}} \int_a^b e^{-i2\pi n \omega} g(\omega) d\omega \right\}.$$

But $\cos(\pi n(k - k')) = (-1)^{k-k'}$, which provides the simplification of the first term. For the second term, just as in the proof of Proposition 2, we simply do integration by parts as many times as possible on the now standard-form oscillatory integral in the second term to get

$$\int_a^b e^{-2\pi i n \omega} g(\omega) d\omega = - \sum_{j=0}^{m-1} (-2\pi i n)^{-j-1} \left\{ g^{(j)}(b) e^{-2\pi i n b} - g^{(j)}(a) e^{-2\pi i n a} \right\} + \mathcal{O}(n^{-m-1}).$$

An elementary rearrangement gives the result. \square

While this proposition is presented in generality, there is a reasonable amount of additional simplification that one can do with the right-hand side based on the value of $k + k' \pmod{4}$. In particular, we see that $e^{i\pi n(k+k')/2} = i^{k-k' \pmod{4}}$, which means that every single complex exponential in the right-hand side of (3.5) simplifies nicely. If we assume that $k = k' \pmod{4}$ so that $e^{i\pi n(k+k')/2} = 1$, the asymptotic expansion term can be more concretely expanded to

$$\begin{aligned} & \Re \left\{ (\cos(2\pi b) + i \sin(2\pi b)) \sum_{j=0}^{m-1} \frac{g^{(j)}(b)}{(-i2\pi n)^{j+1}} - (\cos(2\pi a) + i \sin(2\pi a)) \sum_{j=0}^{m-1} \frac{g^{(j)}(a)}{(-i2\pi n)^{j+1}} \right\} \\ &= \cos(2\pi b) \sum_{j=0, j \text{ odd}}^{m-1} (-1)^{1+|j/2|} \frac{g^{(j)}(b)}{(2\pi n)^{j+1}} - \cos(2\pi a) \sum_{j=0, j \text{ odd}}^{m-1} (-1)^{1+|j/2|} \frac{g^{(j)}(a)}{(2\pi n)^{j+1}} \\ &+ \sin(2\pi b) \sum_{j=0, j \text{ even}}^{m-1} (-1)^{2+|j/2|} \frac{g^{(j)}(b)}{(2\pi n)^{j+1}} - \sin(2\pi a) \sum_{j=0, j \text{ even}}^{m-1} (-1)^{2+|j/2|} \frac{g^{(j)}(a)}{(2\pi n)^{j+1}}. \end{aligned}$$

And while we don't enumerate the other cases for the three values of $e^{i\pi n(k+k')/2}$, the only difference is in the odd/even indexing and the alternating sign inside the sum. The key takeaway here is that the entire integral (3.2) can actually be written as a very smooth integral term ($\int_a^b g(\omega) d\omega$), four trigonometric functions that are non-oscillatory since they have unit wavelength and $a, b \in [-1/2, 1/2]$ with coefficients taken from functions that are themselves smooth (since $g \in \mathcal{C}^{(m)}([a, b])$), and a remainder term depending on high-order derivatives of $g(\omega)$ on $[a, b]$. As it pertains to the Whittle correction matrix \mathbf{C} , for each of the Type-I regions we have endpoints $(a = -1/2, b = \omega_k - \gamma)$, $(a = \omega_k + \gamma, b = \omega_{k'} - \gamma)$, and $(a = \omega_{k'} + \gamma, b = 1/2)$ respectively, and so the effective contribution of the Type-I integrals to $\mathbf{C}_{k,k'}$ is given by $\int_{[-1/2, 1/2] \setminus (B_\gamma(\omega_k) \cup B_\gamma(\omega_{k'}))} \tilde{S}_{n,k,k'}(\omega) d\omega$ and a total of 12 trigonometric functions at the three sets of given endpoints a and b with smoothly varying coefficients. Given that the trigonometric functions are analytic and that $g \in \mathcal{C}^{(m)}([-1/2, 1/2])$, since very smooth kernel matrices often exhibit rapid spectral decay (an observation dating back to at least [18] with the Fast Multipole Method (FMM)), we expect the contribution of the Type-I intervals to \mathbf{C} to have exceptionally fast spectral decay and be severely rank-deficient so long as the remainder from the asymptotic expansion is small. With slightly more effort, we may repeat this analysis on the Type-II regions with singularities.

For the first Type II region of $[\omega_k - \gamma, \omega_k + \gamma]$, the story is only slightly more complicated. This time we introduce the condensed notation of

$$\tilde{S}_{n,k'}(\omega) = \csc(\pi(\omega_{k'} - \omega))(S(\omega) - S(\omega_k))$$

for the bounded and non-oscillatory part of the integrand, and we study

$$\int_{\omega_k + \gamma}^{\omega_k - \gamma} \sin(\pi n(\omega_k - \omega)) \sin(\pi n(\omega_{k'} - \omega)) \csc(\pi(\omega_k - \omega)) \tilde{S}_{n,k'}(\omega) d\omega. \quad (3.6)$$

The important observation to make here is that the singularity presented by $\csc(\pi(\omega_k - \omega))$ is simple. Recalling the Laurent expansion $\csc(t) = t^{-1} + \frac{t}{6} + \frac{7t^2}{360} + \dots$, we see that one can simply “subtract off” the singularity and obtain a standard power-series type representation of $\csc(t) - t^{-1} \approx P_l(t)$ for $t \in [-\gamma, \gamma]$ and some low-order polynomial P_l based on the Laurent series. This motivates the decomposition of (3.6) into

$$\begin{aligned} & \int_{\omega_k + \gamma}^{\omega_k - \gamma} \sin(\pi n(\omega_k - \omega)) \sin(\pi n(\omega_{k'} - \omega)) P_l(\omega_k - \omega) \tilde{S}_{n,k'}(\omega) d\omega \\ & + \int_{\omega_k + \gamma}^{\omega_k - \gamma} \sin(\pi n(\omega_k - \omega)) \sin(\pi n(\omega_{k'} - \omega)) \frac{\tilde{S}_{n,k'}(\omega)}{\omega_k - \omega} d\omega. \end{aligned}$$

The first term above can again be expanded as a small number of unit-wavelength trigonometric functions via Proposition 3 with $g(\omega) = P_l(\omega_k - \omega) \tilde{S}_{n,k'}(\omega)$. Because $\tilde{S}_{n,k'}(\omega) = 0$ at $\omega = \omega_k$ and has been assumed to be smooth, the second term is also not singular and is a standard oscillatory integral. Another application of Proposition 3 with $g(\omega) = (\omega_k - \omega)^{-1} \tilde{S}_{n,k'}(\omega)$ can be applied, making the entire contribution of (3.6) expressible as a linear combination of a small number of unit-wavelength trigonometric functions with smoothly varying coefficients.

The final segment of $[-1/2, 1/2]$ to study is the Type II region $[\omega_{k'} - \gamma, \omega_{k'} + \gamma]$, where the singularity caused by $\csc(\pi(\omega_{k'} - \omega))$ has not already been factored out. Introducing one final condensed integrand notation of

$$\tilde{S}_{n,k}(\omega) = \csc(\pi(\omega_k - \omega))(S(\omega) - S(\omega_k)),$$

we again decompose the contribution of that segment as

$$\begin{aligned} & \int_{\omega_{k'} + \gamma}^{\omega_{k'} - \gamma} \sin(\pi n(\omega_k - \omega)) \sin(\pi n(\omega_{k'} - \omega)) \csc(\pi(\omega_{k'} - \omega)) \tilde{S}_{n,k}(\omega) d\omega \\ & = \int_{\omega_{k'} + \gamma}^{\omega_{k'} - \gamma} \sin(\pi n(\omega_k - \omega)) \sin(\pi n(\omega_{k'} - \omega)) P_l(\omega_{k'} - \omega) \tilde{S}_{n,k}(\omega) d\omega \\ & + \int_{\omega_{k'} + \gamma}^{\omega_{k'} - \gamma} \sin(\pi n(\omega_k - \omega)) \sin(\pi n(\omega_{k'} - \omega)) \frac{\tilde{S}_{n,k}(\omega)}{\omega_{k'} - \omega} d\omega. \end{aligned}$$

The first term in the divided integral can be handled yet again by Proposition 3 just as above. The only new wrinkle is that the second term in the right-hand side now still has a singularity. To handle this last term, recall the elementary trick that, for simple singular integrals of smooth functions, one can again subtract off the singularity in the sense of

$$\int_a^b x^{-1} g(x) dx = \int_a^b x^{-1} (g(x) - g(0)) dx + g(0) \log \left| \frac{b}{a} \right|,$$

where $0 \in (a, b)$, $g(x)$ is differentiable at zero, and the logarithmic term is the result of a Cauchy principal-value interpretation of the integral. With this trick in mind, we just split that last term one more time to obtain

$$\begin{aligned} & \int_{\omega_{k'} + \gamma}^{\omega_{k'} - \gamma} \sin(\pi n(\omega_k - \omega)) \sin(\pi n(\omega_{k'} - \omega)) \frac{\tilde{S}_{n,k}(\omega)}{\omega_{k'} - \omega} d\omega \\ & = \int_{\omega_{k'} + \gamma}^{\omega_{k'} - \gamma} \sin(\pi n(\omega_k - \omega)) \sin(\pi n(\omega_{k'} - \omega)) \frac{\tilde{S}_{n,k}(\omega) - \tilde{S}_{n,k}(\omega_{k'})}{\omega_{k'} - \omega} d\omega \\ & + \tilde{S}_{n,k}(\omega_{k'}) \int_{\omega_{k'} + \gamma}^{\omega_{k'} - \gamma} \sin(\pi n(\omega_k - \omega)) \sin(\pi n(\omega_{k'} - \omega)) \frac{1}{\omega_{k'} - \omega} d\omega. \end{aligned}$$

Now that the singularity has been removed, the first term on the right-hand side can once again be expressed as the usual small sum of unit-length trigonometric functions via Proposition 3. With only a slightly more technical application of the singularity subtraction trick, the final term can be written in the Cauchy principle value sense as a sum of a small number of logarithmic terms including ω_k , $\omega_{k'}$, and γ , although we omit the full expression due to its length.

Combining all of these segmented contributions, we finally conclude in representing $\mathbf{C}_{k,k'}$ as a small number of very smooth functions. And while ostensibly breaking the integral into five pieces, two of which need to be broken up again into two or three additional terms to be suitable for expansion, should lead to so many smooth terms that the matrix is not particularly rank-deficient, we note that all of these trigonometric functions have unit wavelength and are potentially linearly dependent with each other, and that derivatives of the corresponding function g in each application of Proposition 3 are by supposition also well-behaved. As we show in the numerical demonstrations section, for sufficiently well-behaved spectral densities S one can go from three correct digits with a diagonal approximation to 14 correct digits with only a rank $r = 2$ approximation to \mathbf{C} , even when $\mathbf{\Sigma} \in \mathbb{R}^{10^5 \times 10^5}$. And even for less well-behaved $S(\omega)$, such as one with no derivatives at the origin, a rank of $r = 128$ is sufficient for 14 digits even for a $\mathbf{\Sigma}$ of the same size.

This derivation is also illuminating about the sources of error in Whittle approximations and the degree of rank-structure in the Whittle correction matrices. For example, if S has rough points where it is continuous but not smooth, then the above domain partitioning will have to be refined so that Corollary 1 can be applied to fix the accuracy of the asymptotic approximation. This will then mean that $\mathbf{C}_{k,k'}$ will need more asymptotic expansion-sourced terms for the expansion to be accurate. Moreover, we see that if the remainder term in the asymptotic expansion is large, there is potentially a great deal of structure in that matrix that this examination does not account for. One such setting where that can easily happen is when $S(\omega)$ itself is highly oscillatory. As an example, a frustrating challenge for many fast matrix methods is the triangular covariance function with a large bandwidth, such as $h_k = \max(0, 1 - |k|/r)$ with large r . Picking $r = 3n/4$ will provide a $\mathbf{\Sigma}$ that is likely to be problematic for hierarchical matrix-type methods because it is zero on the outer triangles of the largest off-diagonal $n/2 \times n/2$ blocks, making low-rank approximations for them impossible (or at least inaccurate). That problem can also be observed in the spectral domain, as the corresponding spectral density to that sequence $\{h_k\}$ is $S(\omega) = \frac{\sin(2\pi r\omega/2)^2}{r \sin(2\pi\omega/2)^2}$. The problem with this SDF is that its derivatives $S^{(j)}(\omega)$, while smooth, are highly oscillatory. This will make both the asymptotic expansion terms themselves contribute more non-negligible structure to \mathbf{C} as well as produce a significant remainder term $\int_{-1/2}^{1/2} S^{(m)}(\omega) e^{2\pi i\omega(k-k')} d\omega$ that is not accounted for in the asymptotic expansion. This makes any practical order of asymptotic expansion inaccurate, and leads to Whittle correction matrices \mathbf{C} that do not have favorable spectral decay.

As a final note on the structure being exploited here, it is interesting to consider the Whittle correction matrix \mathbf{C} in the context of other fast algorithms for special matrix-vector products. Particularly after subtracting off singularities, one may view \mathbf{C} as a kernel matrix made with a bandlimited function, which is precisely the type of structure that is exploited in existing methods like the fast sinc transform and fast Gauss transform [19, 20]. But unlike in those cases, this compactly supported Fourier transform is highly oscillatory for *every* entry. This is exactly what we exploit here, however, to understand the low-rank structure of \mathbf{C} : *every* entry of \mathbf{C} is the result of a high frequency oscillatory integral of a compactly supported function, and so asymptotic expansion-type methods can be employed equally accurately for every component.

4 Numerical assembly and action of the Whittle correction

With this theoretical justification for the low-rank structure of the Whittle correction matrix, we now turn to discussing how to actually compute and assemble the matrices \mathbf{U} and \mathbf{V} such that $\mathcal{F}\mathbf{\Sigma}\mathcal{F}^H - \mathbf{D} \approx \mathbf{U}\mathbf{V}^H$. First, we note that the action of $\mathbf{\Sigma}$ onto vectors can be done in $\mathcal{O}(n \log n)$ with the familiar circulant embedding technique [33] once the values $\{h_k\}_{k=0}^{n-1}$ have been computed. While we refer readers to the references for a more complete discussion of circulant embedding, we will provide a brief discussion here. The symmetric Toeplitz matrix $\mathbf{\Sigma}$ is specified entirely by its first column $[h_0, h_1, \dots, h_{n-1}]$. This column can be extended to one of length $2n - 1$ given by $\mathbf{c} = [h_0, h_1, \dots, h_{n-1}, h_{n-1}, h_{n-2}, \dots, h_1]$, and if one assembles a Toeplitz matrix with this length $2n - 1$ column the matrix is in fact circulant, which means it is diagonalized by the FFT [17]. Since the FFT can be applied in $\mathcal{O}(n \log n)$ complexity, so can the action of this augmented circulant matrix. Thus, one can compute $\mathbf{\Sigma}\mathbf{v}$ for any vector \mathbf{v} by extracting the first n components of $\mathbf{C}[\mathbf{v}, \mathbf{0}_{n-1}]$, where \mathbf{C} is the circulant matrix made with \mathbf{c} and $\mathbf{0}_{n-1}$ is $n - 1$ many zeros appended to \mathbf{v} .

Letting \mathcal{F}_n be the FFT of size n (briefly now defined without the “fftshift”), we can thus summarize the

action of $\mathcal{F}_n \Sigma \mathcal{F}_n^H - \mathbf{D}$ on a vector \mathbf{v} with

$$(\mathcal{F}_n \Sigma \mathcal{F}_n^H - \mathbf{D})\mathbf{v} = \mathcal{F}_n \left\{ \mathcal{F}_{2n-1}^H \left(\left\{ \mathcal{F}_{2n-1} \mathbf{c} \right\} \circ \mathcal{F}_{2n-1} \begin{bmatrix} \mathcal{F}_n^H \mathbf{v} \\ \mathbf{0}_{n-1} \end{bmatrix} \right) \right\}_{1:n} - \mathbf{D}\mathbf{v}.$$

Assuming that $\mathcal{F}_{2n-1} \mathbf{c}$ is pre-computed, this means that the action of $\mathcal{F} \Sigma \mathcal{F}^H - \mathbf{D}$ on \mathbf{v} requires four FFTs, two of size n and two of size $2n - 1$.

With this established, we turn to the process of approximating \mathbf{C} from the position of only being able to apply it to vectors efficiently. The field of randomized low-rank approximations has become an important part of modern numerical linear algebra, and we refer readers to review papers like [21] and the more recent [31] for broad introductions and context. As it pertains to this work, it is sufficient to discuss the problem of using randomized algorithms to estimate the range of a matrix. Letting $\mathbf{A} \in \mathbb{R}^{n \times n}$ denote an arbitrary matrix of rank r , [21] shows that the orthogonal matrix \mathbf{Q} such that

$$\mathbf{A}\mathbf{\Omega} = \mathbf{Q}\mathbf{R},$$

where $\mathbf{\Omega} \in \mathbb{R}^{n \times (r+p)}$ is a ‘‘sketching’’/test matrix, which in this work will be made of i.i.d. standard normal random variables (although other and potentially faster choices are available), is an approximate basis for the column space of \mathbf{A} . Here p is an oversampling parameter which is often picked to be some small number like $p = 5$. From there, one obtains a simple low-rank representation of \mathbf{A} as

$$\mathbf{A} \approx \underbrace{\mathbf{Q}}_{\mathbf{U}} \underbrace{\mathbf{Q}^H \mathbf{A}}_{\mathbf{V}^H}.$$

This low-rank representation can easily be converted to other truncated factorization types like a partial SVD or eigendecomposition (the representation used in the software implementation of this paper) [21]. Connecting this to Section 2, then, we see that obtaining a rank r approximation $\mathcal{F} \Sigma \mathcal{F}^H - \mathbf{D}$ requires applying it to $r + p$ many random vectors. While there is sufficient structure in this specific matrix-vector application that one could reduce the number of FFTs from $4(r + p)$, the implementation used in this work does not employ any particular optimization of that form and is nonetheless satisfyingly fast for an effectively exact method.

4.1 Approximating the log-likelihood

Armed with this low-rank approximation, one now has all of the pieces for working with

$$\mathcal{F} \Sigma \mathcal{F}^H \approx \mathbf{D} + \mathbf{U}\mathbf{V}^H.$$

Letting

$$2\tilde{\ell}(\boldsymbol{\theta} | \mathcal{F}\mathbf{y}) = \log |\mathbf{D} + \mathbf{U}\mathbf{V}^H| + (\mathcal{F}\mathbf{y})^H (\mathbf{D} + \mathbf{U}\mathbf{V}^H)^{-1} (\mathcal{F}\mathbf{y}) \approx 2\ell(\boldsymbol{\theta} | \mathbf{y}) \quad (4.1)$$

denote the approximated log-likelihood, we see that, post-assembly of \mathbf{U} and \mathbf{V} , evaluation of $\tilde{\ell}(\boldsymbol{\theta} | \mathbf{v})$ for an arbitrary vector \mathbf{v} is possible in linear complexity. For the log-determinant term, using the matrix determinant lemma we see that

$$\log |\mathbf{D} + \mathbf{U}\mathbf{V}^H| = \log |\mathcal{I}_r + \mathbf{V}^H \mathbf{D}^{-1} \mathbf{U}| + \log |\mathbf{D}|.$$

For the quadratic form, we may compute it using the Sherman-Morrison-Woodbury formula as

$$\mathbf{v}^T (\mathbf{D} + \mathbf{U}\mathbf{V}^H)^{-1} \mathbf{v} = \mathbf{v}^T \mathbf{D}^{-1} \mathbf{v} - \mathbf{v}^T \mathbf{D}^{-1} \mathbf{U} (\mathcal{I}_r + \mathbf{V}^H \mathbf{D}^{-1} \mathbf{U})^{-1} \mathbf{V}^H \mathbf{D}^{-1} \mathbf{v}.$$

Since all of the matrix-matrix operations in the right-hand sides of those two equations are for small $\mathbb{R}^{r \times r}$ matrices, we see that both the log-determinant and the quadratic form can be evaluated in $\mathcal{O}(n)$ complexity. And since the assembly of $\mathbf{D} + \mathbf{U}\mathbf{V}^H$ is done in $\mathcal{O}(n \log n)$, we conclude that the full job of assembling the approximation and then evaluating the approximated log-likelihood runs in quasilinear time complexity and linear storage complexity.

As will be highlighted in the next section, one particularly attractive aspect of this specific approximation structure is that it is very simple. Due to this simplicity, two approximated DFT-conjugated Toeplitz matrices can be exactly multiplied in $\mathcal{O}(n)$ complexity, for example, and even the inverse of one can be applied to the other at the same cost. Let us now discuss how to continue exploiting this structure of $\mathcal{F} \Sigma \mathcal{F}^H$ in obtaining similarly accurate gradients and information matrices for a wide range of models.

4.2 Gradients, factorization, and information matrices

If one assumes that a parametrically indexed spectral density $S_{\boldsymbol{\theta}}(\omega)$ has partial derivatives $\partial_{\theta_j} S_{\boldsymbol{\theta}}(\omega)$ that share the same smoothness structure as $S_{\boldsymbol{\theta}}$ with respect to ω (such as being piecewise $\mathcal{C}^{(m)}([-1/2, 1/2])$), then the above arguments about the low-rank structure of $\mathcal{F}\boldsymbol{\Sigma}\mathcal{F}^H$ apply equally well to $\mathcal{F}\{\partial_{\theta_j}\boldsymbol{\Sigma}\}\mathcal{F}^H$. For notational clarity, throughout this section we absorb the DFT matrix \mathcal{F} into $\boldsymbol{\Sigma}$ and write all equations without the many conjugations with \mathcal{F} , commenting on it only in places where it materially affects computations or does not completely cancel out.

To start, we introduce the subscript j and let \mathbf{D}_j , \mathbf{U}_j , and \mathbf{V}_j be matrices such that

$$\mathcal{F}\left\{\frac{\partial}{\partial\theta_j}\boldsymbol{\Sigma}(\boldsymbol{\theta})\right\}\mathcal{F}^H \approx \mathbf{D}_j + \mathbf{U}_j\mathbf{V}_j^H. \quad (4.2)$$

The j -th term of the gradient of the Gaussian negative log-likelihood $\ell(\boldsymbol{\theta}; \mathbf{y})$ is given by

$$2[\nabla\ell(\boldsymbol{\theta} | \mathbf{y})]_j = \text{tr}\left(\boldsymbol{\Sigma}(\boldsymbol{\theta})^{-1}\left\{\frac{\partial}{\partial\theta_j}\boldsymbol{\Sigma}(\boldsymbol{\theta})\right\}\right) - \mathbf{y}^H\boldsymbol{\Sigma}(\boldsymbol{\theta})^{-1}\left\{\frac{\partial}{\partial\theta_j}\boldsymbol{\Sigma}(\boldsymbol{\theta})\right\}\boldsymbol{\Sigma}(\boldsymbol{\theta})^{-1}\mathbf{y}. \quad (4.3)$$

Observing this equivalent structure in (4.2), we note that the quadratic form term in (4.3) can easily be evaluated in $\mathcal{O}(n)$ complexity once the two low-rank approximations have been assembled by again making use of the Sherman-Morrison-Woodbury formula and the speed of simple matrix-vector products. More interesting, however, and what sets this approximation method apart from more complex general-purpose matrix compression methods is that the trace can also be computed exactly without resorting to stochastic trace estimation (see [15] and references therein for discussion). In particular, note that the Sherman-Morrison-Woodbury formula given in the above section implies that $(\mathbf{D} + \mathbf{U}\mathbf{V}^H)^{-1}$ can be again represented as a low rank perturbation of a diagonal matrix, which we will denote as $\tilde{\mathbf{D}} + \tilde{\mathbf{U}}\tilde{\mathbf{C}}\tilde{\mathbf{V}}^H$. Applying this, we see that

$$\begin{aligned} (\mathbf{D} + \mathbf{U}\mathbf{V}^H)^{-1}(\mathbf{D}_j + \mathbf{U}_j\mathbf{V}_j^H) &= (\tilde{\mathbf{D}} + \tilde{\mathbf{U}}\tilde{\mathbf{C}}\tilde{\mathbf{V}}^H)(\mathbf{D}_j + \mathbf{U}_j\mathbf{V}_j^H) \\ &= \tilde{\mathbf{D}}\mathbf{D}_j + \tilde{\mathbf{D}}\mathbf{U}_j\mathbf{V}_j^H + \tilde{\mathbf{U}}\tilde{\mathbf{C}}\tilde{\mathbf{V}}_H^H\mathbf{D}_j + \tilde{\mathbf{U}}\tilde{\mathbf{C}}\tilde{\mathbf{V}}^H\mathbf{D}_j + \mathbf{U}_j\mathbf{V}_j^H \\ &= \tilde{\mathbf{D}}\mathbf{D}_j + \mathbf{M}. \end{aligned}$$

While this looks problematic, we note that the matrix \mathbf{M} defined as the last three terms in the above equation is a sum of three matrices whose rank is $\leq r$, and so the rank of \mathbf{M} is at most $3r$. Second, because each of those terms is already a low-rank representation that can be applied to vectors in $\mathcal{O}(n)$ time, we can simply repeat the randomized low-rank approximation strategy from earlier, computing first a randomized basis for the column space with

$$(\tilde{\mathbf{D}}\mathbf{U}_j\mathbf{V}_j^H + \tilde{\mathbf{U}}\tilde{\mathbf{C}}\tilde{\mathbf{V}}_H^H\mathbf{D}_j + \tilde{\mathbf{U}}\tilde{\mathbf{C}}\tilde{\mathbf{V}}^H\mathbf{D}_j + \mathbf{U}_j\mathbf{V}_j^H)\boldsymbol{\Omega} = \mathbf{Q}\mathbf{R}$$

and then re-compressing to a single low-rank representation with $\mathbf{Q}\mathbf{Q}^H\mathbf{M}$. From there, we observe the simple fact that $\text{tr}(\mathbf{A} + \mathbf{B}\mathbf{C}^T) = \text{tr}(\mathbf{A}) + \text{tr}(\mathbf{C}^T\mathbf{B})$ and conclude that the trace in (4.3) can be computed exactly and in $\mathcal{O}(n)$ time. As will be demonstrated in the next section, these gradients are computed to similarly high accuracy as the log-likelihood evaluation itself, providing effectively the same number of digits.

A second pleasant property of this approximation structure for $\boldsymbol{\Sigma}$ is that it admits a simple and direct symmetric factorization. In the above discussions for notational simplicity we have worked with the low rank form $\mathbf{D} + \mathbf{U}\mathbf{V}^H$. But as previously mentioned, these low-rank representations can be easily and quickly converted to other structures like a partial SVD or eigendecomposition [21]. For this factorization, it is easiest to work with a representation like $\mathbf{D} + \mathbf{U}\boldsymbol{\Lambda}\mathbf{U}^H$, where $\boldsymbol{\Lambda} \in \mathbb{R}^{r \times r}$ is a diagonal matrix of eigenvalues of the low-rank Whittle correction. In this form, a slight manipulation and then applying Theorem 3.1 of [1] gives a very simple symmetric factorization as

$$\mathbf{D} + \mathbf{U}\boldsymbol{\Lambda}\mathbf{U}^H = \mathbf{D}^{1/2}(\mathcal{I} + \tilde{\mathbf{U}}\boldsymbol{\Lambda}\tilde{\mathbf{U}}^H)\mathbf{D}^{1/2} = \mathbf{D}^{1/2}(\mathcal{I} + \tilde{\mathbf{U}}\mathbf{X}\tilde{\mathbf{U}}^H)(\mathcal{I} + \tilde{\mathbf{U}}\mathbf{X}\tilde{\mathbf{U}}^H)^H\mathbf{D}^{1/2} = \mathbf{W}\mathbf{W}^H,$$

where $\tilde{\mathbf{U}} = \mathbf{D}^{-1/2}\mathbf{U}$ and $\mathbf{X} = \mathbf{L}^{-H}(\mathbf{M} - \mathcal{I})\mathbf{L}^{-1}$, $\mathbf{U}^T\mathbf{U} = \mathbf{L}\mathbf{L}^T$, and $\mathcal{I} + \mathbf{L}^T\boldsymbol{\Lambda}\mathbf{L} = \mathbf{M}\mathbf{M}^T$. While that is many equations, the actual computation of the matrix \mathbf{X} used in assembling \mathbf{W} is done in just a few $\mathbb{R}^{r \times r}$ matrix-matrix operations (Algorithms 1 and 2 in [1]).

This symmetric factor is useful for several purposes. For one, it gives a means of obtaining exact simulations of any time series in $\mathcal{O}(n \log n)$ time, although of course standard periodic embedding would be a more simple and efficient way of achieving the same thing. In the setting of derivative information, it offers a more novel benefit in that it enables very accurate stochastic estimation of Fisher information matrices.

The Fisher information matrix for parameters $\boldsymbol{\theta}$ in a Gaussian model like the one used in this work is given by, again in terms of just $\boldsymbol{\Sigma}(\boldsymbol{\theta})$,

$$\mathbf{I}(\boldsymbol{\theta})_{j,k} = \frac{1}{2} \text{tr} \left(\boldsymbol{\Sigma}(\boldsymbol{\theta})^{-1} \left\{ \frac{\partial}{\partial \theta_j} \boldsymbol{\Sigma}(\boldsymbol{\theta}) \right\} \boldsymbol{\Sigma}(\boldsymbol{\theta})^{-1} \left\{ \frac{\partial}{\partial \theta_k} \boldsymbol{\Sigma}(\boldsymbol{\theta}) \right\} \right). \quad (4.4)$$

This matrix is the asymptotic precision of the MLE under sufficient regularity conditions, and is often substituted in place of the Hessian matrix of a log-likelihood $\ell(\boldsymbol{\theta})$ due to the fact that it is easier to compute and is always positive definite. As discussed above, it is fully possible to scalably evaluate this sequence of matrix-matrix products to obtain an exact Fisher information matrix, and in the following section we will provide a verification that this computation still runs in quasilinear complexity despite the large number of matrix-matrix operations. But [15] introduced a fast “symmetrized” stochastic estimator for the matrix $\mathbf{I}(\boldsymbol{\theta})$ that is very accurate and can be computed in a fraction of the runtime cost of the exact $\mathbf{I}(\boldsymbol{\theta})$. Stochastic trace estimation is a rich field with a broad literature (we refer readers to [4] for a useful introduction and overview), but for this work the fundamental observation to make is that for any random vector \mathbf{u} with $\mathbb{E}\mathbf{u} = \mathbf{0}$ and $\mathbb{V}\mathbf{u} = \mathcal{I}$, we have that $\mathbb{E}\mathbf{u}^T \mathbf{A} \mathbf{u} = \text{tr}(\mathbf{A})$ for any matrix \mathbf{A} . The *sample average approximation* (SAA) trace estimator is then based on drawing several i.i.d. vectors \mathbf{u} , denoted $\{\mathbf{u}_j\}_{j=1}^M$, and instead of evaluating the trace directly using

$$M^{-1} \sum_{j=1}^M \mathbf{u}_j^T \mathbf{A} \mathbf{u}_j \approx \text{tr}(\mathbf{A}).$$

The variance of this estimator depends on several properties of \mathbf{A} , but a specific choice of \mathbf{u} having i.i.d. random signs is particular popular because $\mathbb{V}\mathbf{u}^T \mathbf{A} \mathbf{u} = 2(\|\mathbf{A}\|_F^2 - \sum_j A_{j,j}^2)$, so that for diagonally concentrated matrices this estimator can be quite accurate.

Stochastic trace estimation has been applied to the Gaussian process computation problem in many works, notably first in [3]. In [27], a theorem was provided indicating that if $\boldsymbol{\Sigma} = \mathbf{W}\mathbf{W}^T$, then using the simple property that $\text{tr}(\mathbf{A}\mathbf{B}) = \text{tr}(\mathbf{B}\mathbf{A})$ combined with this factorization one can instead compute $\mathbf{I}_{j,k}$ with

$$\mathbf{I}_{j,k} = \frac{1}{2} \text{tr} \left(\mathbf{W}^{-T} \left\{ \frac{\partial}{\partial \theta_j} \boldsymbol{\Sigma}(\boldsymbol{\theta}) \right\} \boldsymbol{\Sigma}(\boldsymbol{\theta})^{-1} \left\{ \frac{\partial}{\partial \theta_k} \boldsymbol{\Sigma}(\boldsymbol{\theta}) \right\} \mathbf{W}^{-1} \right), \quad (4.5)$$

and the variance of the SAA estimator for (4.5) is bounded above by the variance of the SAA estimator for (4.4). This theoretical observation was verified in [15] and subsequent works, and [15] provided an even further “symmetrized” trace to estimate for off-diagonal elements. Introducing the notation $\boldsymbol{\Sigma}_j = \partial_{\theta_j} \boldsymbol{\Sigma}(\boldsymbol{\theta})$, one may compute a fully “symmetrized” trace with

$$\widehat{\mathbf{I}}_{j,k} = (4M)^{-1} \sum_{l=1}^M \mathbf{u}_l^T \mathbf{W}^{-1} (\boldsymbol{\Sigma}_j + \boldsymbol{\Sigma}_k) \boldsymbol{\Sigma}^{-1} (\boldsymbol{\Sigma}_j + \boldsymbol{\Sigma}_k) \mathbf{W}^{-T} \mathbf{u}_l - \frac{1}{2} \widehat{\mathbf{I}}_{j,j} - \frac{1}{2} \widehat{\mathbf{I}}_{k,k}, \quad (4.6)$$

where diagonal elements $\mathbf{I}_{j,j}$ are trivial to fully symmetrize and thus can be computed in advance of the off-diagonal ones.

This estimator $\widehat{\mathbf{I}}$ enjoys both very high accuracy and great computational benefits. The primary computational benefit is that this can be computed in a single pass over the derivative matrices $\boldsymbol{\Sigma}_j$, since all one needs to evaluate (4.6) is $\boldsymbol{\Sigma}^{-1}$ and $\{\boldsymbol{\Sigma}_j \mathbf{W}^{-T} \mathbf{u}_l\}_{l=1}^M$. Since one commonly uses $M \approx 70$ or some similarly small number of SAA vectors, for example, it is very easy to pre-solve the SAA vectors $\{\mathbf{u}_l\}$ with \mathbf{W}^{-T} and then in a single for-loop assemble and apply $\boldsymbol{\Sigma}_j$ to each of them. Whether those pre-applied vectors are saved to disk or kept in RAM, there is no more need for derivative matrices $\boldsymbol{\Sigma}_j$ after that point, and so one need not ever even have $\boldsymbol{\Sigma}_j$ and $\boldsymbol{\Sigma}_k$ instantiated at the same time to fully evaluate $\widehat{\mathbf{I}}$. For models with many parameters, the speedup that this affords can be substantial.

The Hessian of $\ell(\boldsymbol{\theta} | \mathbf{y})$, while again absolutely computable in $\mathcal{O}(n \log n)$ complexity, is a similar situation to the expected Fisher information matrix. It has terms given by (again using just $\boldsymbol{\Sigma}$ instead of $\mathcal{F}\boldsymbol{\Sigma}\mathcal{F}^H$)

$$[H\ell(\boldsymbol{\theta} | \mathbf{y})]_{j,k} = \mathbf{I}_{j,k} + \text{tr}(\boldsymbol{\Sigma}^{-1} \{ \partial_{\theta_k} \partial_{\theta_j} \boldsymbol{\Sigma} \}) - \mathbf{y}^H (\partial_{\theta_k} \{ \boldsymbol{\Sigma}^{-1} \boldsymbol{\Sigma}_j \boldsymbol{\Sigma}^{-1} \}) \mathbf{y}.$$

From this expression one sees that the same things are possible as with the gradient, but the prefactor on all operations will be larger: one must compute and re-compress matrix products involving second derivatives of $\mathbf{D} + \mathbf{U}\mathbf{V}^H$ with respect to model parameters, and one must again do a full matrix-matrix multiply for the additional trace (unless one opts to again use SAA). All of these things are perfectly computable using the tools already introduced in this work. But because of the high prefactor cost, we do not explore them further here.

5 Numerical demonstrations

In this section we will demonstrate the efficiency and accuracy of this method for approximating $\boldsymbol{\Sigma}$, the log-likelihood, and its derivatives. In particular, we will study two spectral densities:

$$\begin{aligned} S_1(\omega) &= \theta_1(1 - 2\theta_2 \cos(2\pi\omega) + \theta_2^2)^{-1} \\ S_2(\omega) &= \theta_1 e^{-\theta_2|\omega|}, \end{aligned}$$

which have corresponding autocovariance sequences

$$\begin{aligned} h_{1,k} &= \theta_1(1 - \theta_2^2)^{-1} \theta_2^k \\ h_{2,k} &= \frac{2\theta_1 e^{-\theta_2/2} (-\theta_2 \cos(\pi k) + e^{\theta_2/2} \theta_2 + 2\pi k \sin(\pi k))}{\theta_2^2 + (2\pi k)^2}. \end{aligned}$$

The model S_1 was chosen because it is not only very smooth and with a limited dynamic range, but its periodic extension is even continuous at the endpoints (which the above section demonstrates are often the dominating source of structure in the Whittle correction for otherwise smooth SDFs). This spectral density is in some sense maximally well-behaved, and its corresponding autocovariance sequence decays predictably quickly. From the perspective of this approximation framework, this is an ideal setting. $S_2(\omega)$, on the other hand, is more challenging because of its roughness at the origin. This model was chosen to demonstrate that the directional derivative correction introduced above can fully restore the accuracy of asymptotic expansions even for spectral densities that aren't even always once differentiable, and that the rank structure of \mathcal{C} is still very much exploitable.

As a first investigation, we verify the quasilinear runtime complexity of assembling the matrix approximation and evaluating (4.1). Figure 1 shows the runtime cost of those computations for a variety of data sizes ranging from $n = 1000$ to $n = 96000$ along with a theoretical $\mathcal{O}(n \log n)$ line. As one would expect for a fixed-rank approximation assembled using $\mathcal{O}(1)$ FFTs, the empirical agreement with the theoretical complexity is good. While there is variation in runtime cost when the entire assembly runs in significantly under one second, by the time the program runtime cost approaches a second the stability of the scaling is clear.

As a second investigation, we look at the relative error in the negative log-likelihood computed with the implied approximation to (1). This study, summarized in Figure 2, clearly demonstrates the way that this approximation depends on the specific spectral density being modeled. For S_1 , we see that even a rank of $r = 2$ provides an effectively exact log-likelihood with 14+ digits of precision. The second two sub-plots in Figure 2 show two different applications with S_2 . The center figure shows the relative accuracy of the negative log-likelihood when one does *not* correct the asymptotic expansion for the rough point at the origin when computing the autocovariance sequence $\{h_k\}_{k=0}^{n-1}$, instead simply pretending that the function has many derivatives everywhere. In this work the asymptotic expansions were used for $k > 2000$, and it is clear in the figure that as soon as those expansions start being used that one goes from 14 digits in the rank $r = 128$ case to 8 digits, and the quality of the approximation does not meaningfully improve even as the rank varies by an order of magnitude.

The final panel in Figure 2 shows the relative error of the likelihood approximation (1) with the corrected asymptotic expansion that applies Corollary 1 at the splitting point $\omega_1^r = 0$. Here we now see that there

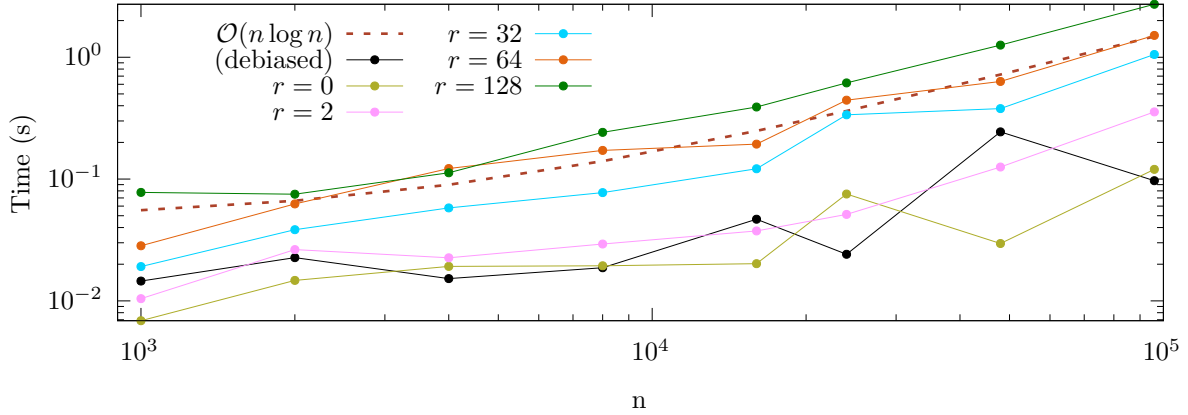


Figure 1: The runtime cost of assembling the approximation $\mathcal{F}\Sigma\mathcal{F}^H \approx \mathbf{D} + \mathbf{U}\mathbf{V}^H$ and evaluating (4.1) for various different ranks r . For additional context, we provide the runtime cost of assembling just the diagonal matrix of $S(\omega)$ at Fourier frequencies ($r = 0$) and the debiased Whittle estimator.

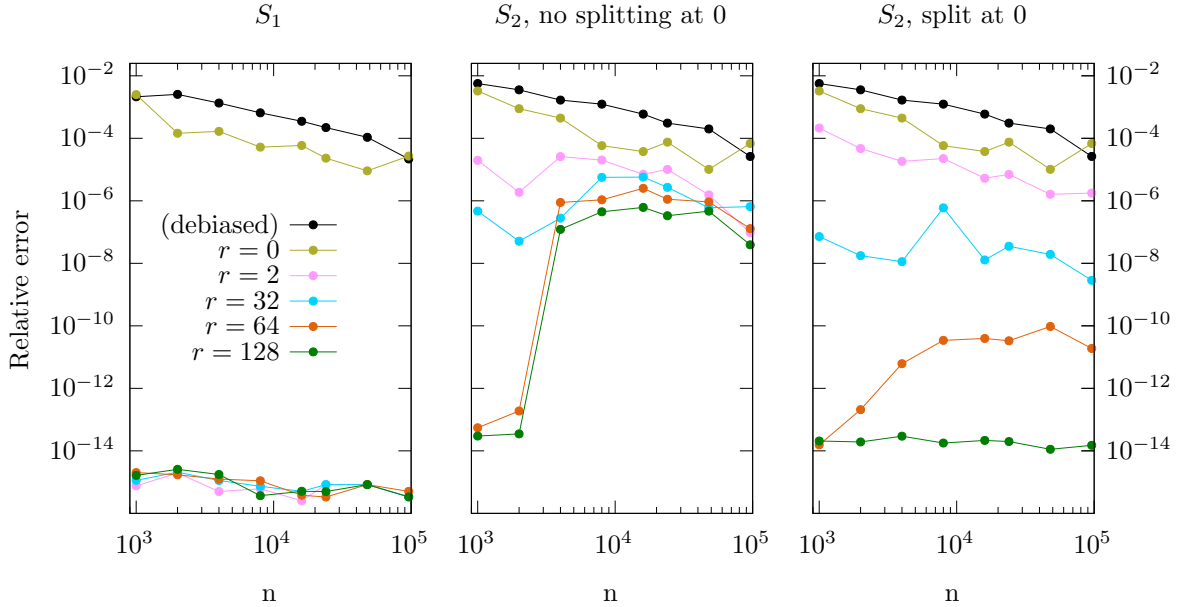


Figure 2: The relative errors in the negative log-likelihood (1) for various models, ranks, and data sizes. The middle column shows the error in naively applying the asymptotic expansion method of Proposition 2 to obtain $\{h_k\}_{k=0}^{n-1}$ despite $S_2(\omega)$ having zero derivatives at the origin, and the right column applies the splitted expansion method from Corollary 1.

is no visible loss in accuracy once the expansions start being used for tails of the autocovariance sequence, indicating that the domain-splitting correction restores the accuracy of the expansions. As the theory would imply and this figure empirically demonstrates, the rank of the “Whittle correction” depends on properties of the spectral density. In this particular case, a rank of $r \approx 100$ is necessary to get almost every significant digit of the log-likelihood. This low rank makes sense in light of Section 3’s asymptotic expansion argument, as $S_2(\omega)$ is non-smooth at the origin and at the periodic endpoints.

Next, we validate the runtime cost and accuracy of the gradient, the exact expected Fisher matrix, and the symmetrized stochastic expected Fisher matrix of the negative log-likelihood, although due to the exact values requiring matrix-matrix products we now only test to matrices of size 48 000. Figure 3 provides a

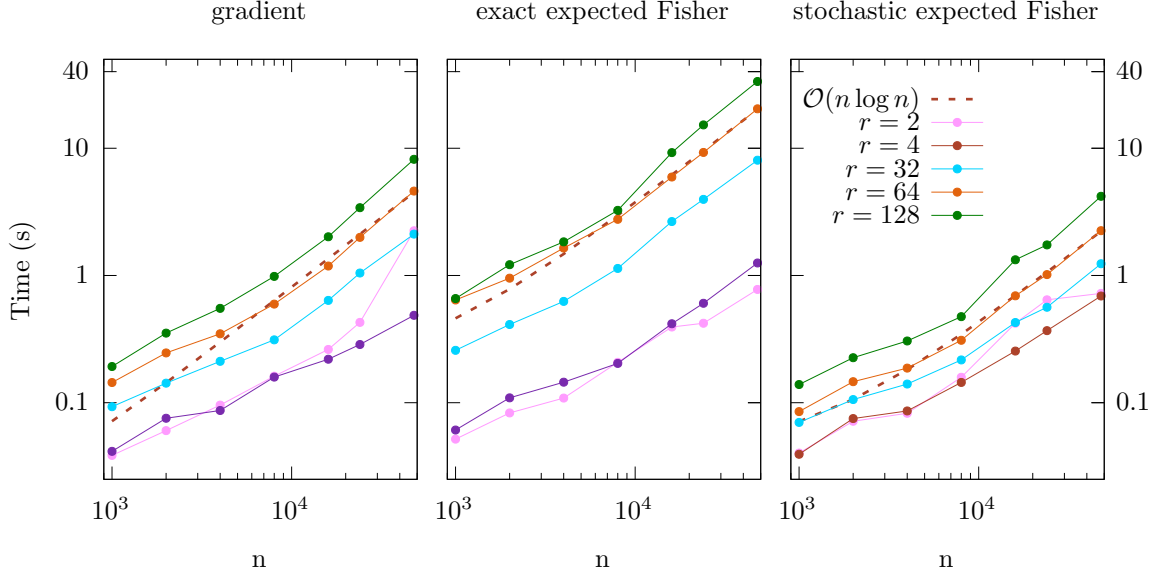


Figure 3: Runtime costs for evaluating the approximated gradient (4.3), the exact Fisher information matrix (4.4), and the symmetrized stochastic expected Fisher information matrix for various data sizes and ranks using $S_2(\omega)$ with asymptotic expansions split at 0.

summary of the runtime cost of computing the three quantities. As can be seen, the agreement with the theoretically expected $\mathcal{O}(n \log n)$ is clear. And even for $n \approx 50\,000$ data points, we see that the gradient of the likelihood—which requires a matrix-matrix product for each term—can be computed to full precision in under ten seconds. By virtue of requiring only matrix-vector products, which are exceptionally fast with this simple low-rank structure, the symmetrized stochastic expected Fisher information matrix is actually slightly faster to compute than the gradient. Each term of the exact expected Fisher information matrix requires a product of four matrices, and so the prefactor of the $\mathcal{O}(n \log n)$ complexity is significantly higher, with the rank $r = 128$ value for $n = 48\,000$ taking about 40 seconds compared to the ≈ 5 s that its stochastic counterpart required. This is of course more expensive, but it is also sufficiently manageable that one could certainly compute it once to high accuracy to obtain the true asymptotic precision of the MLE once the estimate $\hat{\theta}^{\text{MLE}}$ has been computed, for example.

To study the accuracy of these approximations, Figure 4 shows two quantities. Letting $\mathbf{g}(\boldsymbol{\theta})$ denote the true gradient $\nabla \ell(\boldsymbol{\theta} | \mathbf{y})$ and $\tilde{\mathbf{g}}(\boldsymbol{\theta})$ denote the approximated gradient $\nabla \tilde{\ell}(\boldsymbol{\theta} | \mathbf{y})$, the top row shows a standard max-norm type metric of

$$\max_{j=1, \dots, p} \frac{|g_j(\boldsymbol{\theta}) - \tilde{g}_j(\boldsymbol{\theta})|}{|g_j(\boldsymbol{\theta})|}$$

for models $S_1(\omega)$ and $S_2(\omega)$. Letting \mathbf{I} denote the true expected Fisher information matrix and $\tilde{\mathbf{I}}$ denote the approximated one (with just the approximated $\boldsymbol{\Sigma}$ or additionally by using the stochastic trace estimator), the second row of Figure 4 shows the relative operator norm error $\|\mathbf{I}\|^{-1} \|\mathbf{I} - \tilde{\mathbf{I}}\|$, which is arguably a more relevant metric for a Hessian approximation than a pointwise max-norm. Many of the conclusions from examining the relative error in the log-likelihood above still apply here. As before, for spectral density S_1 the matrix $\boldsymbol{\Sigma}$ is so well-behaved that even a rank $r = 4$ approximation to $\mathcal{F}\boldsymbol{\Sigma}\mathcal{F}^H - \mathbf{D}$ and its derivatives gives 12+ digits of accuracy in the gradient and exact expected Fisher matrix. For the likelihood of S_2 , due to the roughness at the origin the rank of the Whittle correction again needs to be increased. But as one would hope, since a rank of $r = 128$ gave effectively every digit in the log-likelihood, it also gives effectively every digit in the gradient and exact expected Fisher matrix. Considering that the derivatives of S_1 and S_2 with respect to θ_2 are not strictly non-negative, this also provides a verification that the structure this method exploits also works well for symmetric Toeplitz matrices that are not positive-definite.

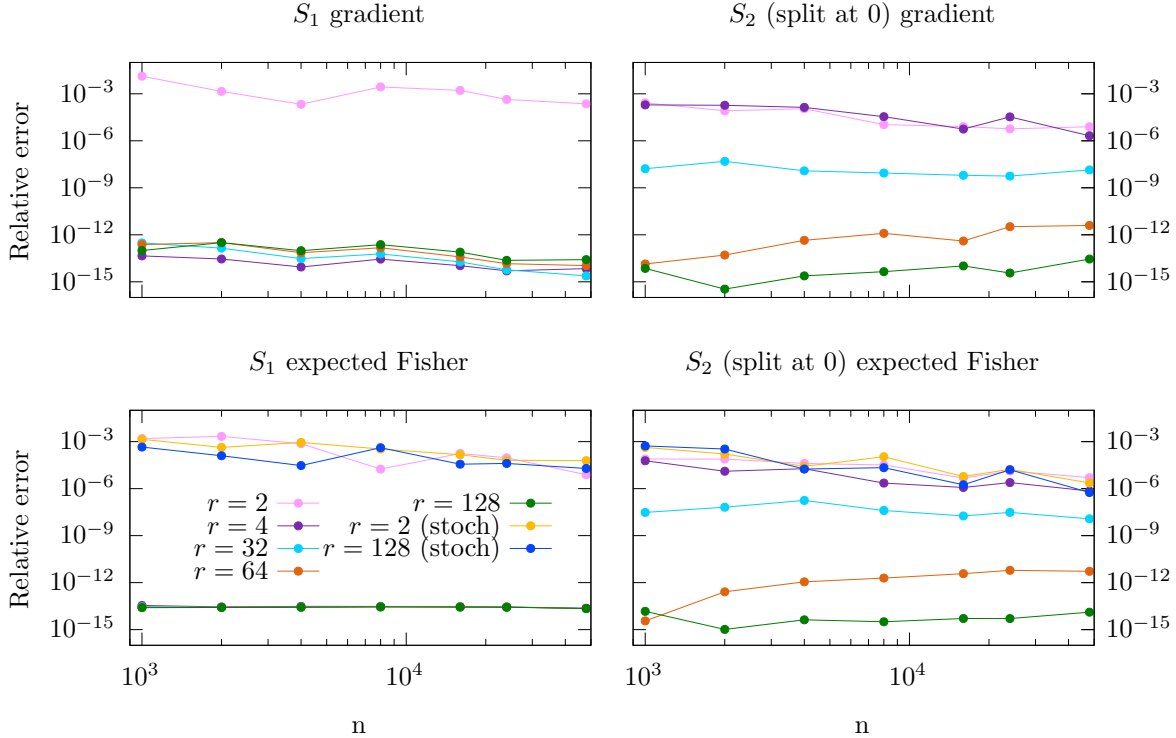


Figure 4: Relative error-type metrics for the approximated gradient and both exact and stochastically approximated Fisher information matrix for various ranks and sizes.

For the stochastic expected Fisher matrix, every trace approximation was done using $M = 72$ SAA vectors and the SAA-induced error is clearly the dominant source of disagreement with the true expected Fisher matrix, even for $r = 2$. While it is tempting to conclude that one could simply set $r = 2$ and obtain a good estimator for the expected Fisher information matrix in under a second even for $n = 50\,000$ data points, which may well be true in plenty of circumstances, the situation can be slightly more complicated than that. When using exact matrices Σ , Σ_j , and Σ_k , the symmetrized stochastic estimator is an unbiased estimator. And while the SAA-induced variability in the approximated expected Fisher using the *matrix* approximation here may be much larger than the bias induced by setting the rank r too small, the estimator now having some amount of bias may be a potential source of issues, so we advise practitioners to reduce r from what they deemed necessary for an accurate log-likelihood with caution.

Finally, as the most direct validation of the method, we conduct a simulation study and compare the true MLE with the estimator obtained from direct optimizing our approximation $\tilde{\ell}(\theta | \mathcal{F}\mathbf{y})$ as well as the Whittle and debiased Whittle approximations. Using the spectral density S_2 with true parameters $\theta_1 = 5$ and $\theta_2 = 35$, we simulate 50 trials with $n = 10\,000$ data points and compute each estimator as well as the true MLE, using a rank of $r = 128$ in our method for all trials. Figure 5 summarizes these results and provides several observations. First, as discussed in the introduction, we readily see that $\hat{\theta}^W$ is severely biased. There is not a single case out of 50 in which the Whittle-based estimator for either parameter is greater than the true MLE. And while the variance of the estimator is also quite high, this bias is still likely to make inferential questions impossible. The debiased Whittle-based estimator, on the other hand, does deliver on providing an estimator that does not show meaningful bias. This exceptionally fast estimator comes only at the cost of much larger variability than the true MLE. Finally, we see that the estimator obtained by optimizing our log-likelihood is effectively identical to the true MLE in all cases, with the biggest absolute difference between point estimates being approximately 10^{-3} . Considering that with rank $r = 128$ the approximation is effectively exact for $S_2(\omega)$ (and, as this example demonstrates, this rank-structure is robust to a wide range of parameter values), this is the expected result.

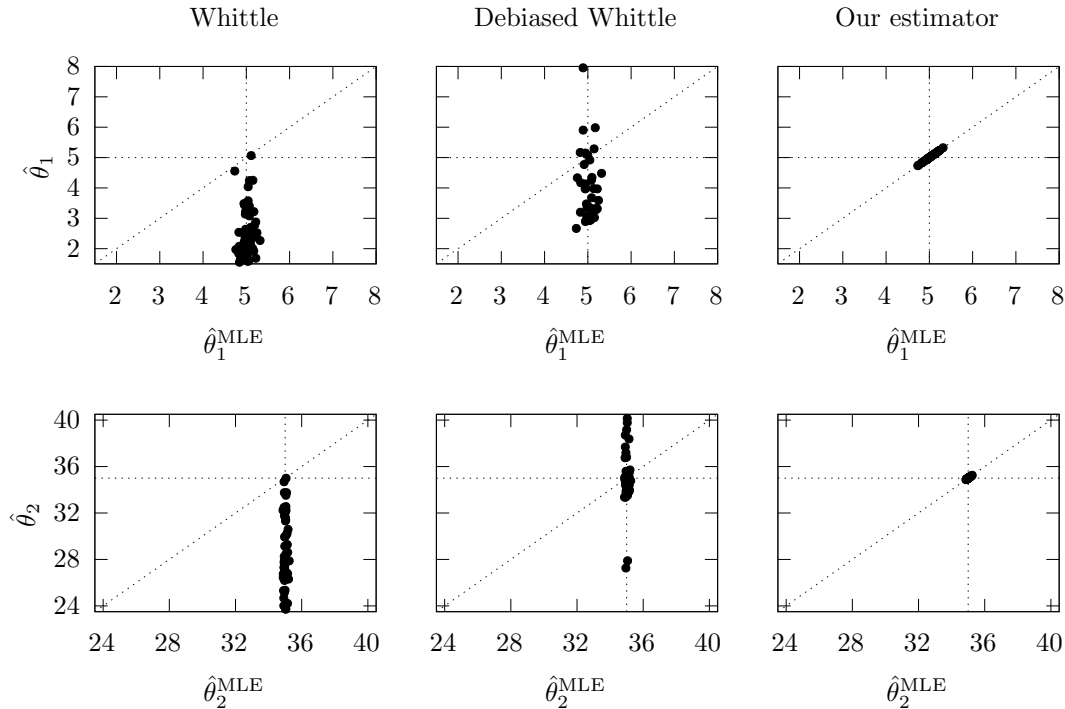


Figure 5: A comparison of the 50 trials of fitting a process simulated with a true SDF of $S_2(\omega)$ with $\theta_1 = 5$ and $\theta_2 = 35$. The first row shows a scatter plot of points $(\hat{\theta}_1^{\text{MLE}}, \hat{\theta}_1)$ with $\hat{\theta}_1$ denoting the alternative estimator, and the lower row shows the analog for the estimates of θ_2 .

6 Discussion

This work introduces a pleasingly simple approximation for the covariance matrix of the DFT of a stationary time series, which incidentally may provide useful methods to a much broader range of settings where one encounters symmetric Toeplitz matrices whose diagonal sequences have well-behaved Fourier transforms. In many settings and more general Gaussian process applications, for example with irregular locations or in multiple dimensions, low rank-type methods are known to have severe limitations [26]. And for purely approximating the Toeplitz matrix Σ , many of those issues would still be present, so it is interesting to observe that conjugating with the DFT matrix changes the algebraic structure of Σ to the degree where a low-rank perturbation of a diagonal matrix represents $\mathcal{F}\Sigma\mathcal{F}^H$ to almost every achievable significant digit at double precision.

The theory in Section 3 provides a new and complementary perspective to existing analyses of the accuracy of Whittle approximations. In [28], for example, a theoretical analysis of spectral-domain approximations is provided where error is characterized by an integer K and the assumption that the corresponding covariance sequence has a finite K -th moment $\sum_j j^K h_j < \infty$. This work, on the other hand, discusses non-smooth points of spectral densities and large high-order derivatives as the principle source of error. These are of course intimately connected, and the correspondence of a function's decay rate with the smoothness of its Fourier transform is well-known. If one is designing parametric models via the spectral density, the considerations that this work motivates for designing models that can be approximated well—namely, selecting and designing the number of non-smooth points, including at endpoints, and deciding on the magnitude of quantities like $\int_{-1/2}^{1/2} S^{(m)}(\omega) e^{2\pi i \omega k} d\omega$ —may be more direct in some circumstances.

Many methods already exist for exploiting structure in covariance matrices like Σ and achieving similar or even slightly better runtime complexity. [10] provides a hierarchically semi-separable-type (HSS) approximation to covariance matrices Σ that runs in linear time, and [14, 15] use hierarchically off-diagonal low-rank structure

(HODLR) to achieve quasilinear complexity that is comparable to that of this work. Many other hierarchical matrix formats exist [8], and in some cases can be pushed to a similar degree of accuracy as the method presented here. What makes this structure representation interesting, in our opinion, is its simplicity. This approximation is easy to implement in software (and the released code can be inspected to prove that point), and the resulting $\mathbf{D} + \mathbf{UV}^H$ has a very transparent structure. Moreover, its runtime complexity is very simple and predictable since it is only controlled by one tuning parameter (the rank r). Despite this, it achieves high accuracy for a very broad class of spectral densities. And for users who are so inclined, making its rank adaptive would be a very simple modification to the code, following, for example, guidelines from [21]. Moreover, error control and analysis for this structure is much more direct than in a more general hierarchical matrix format, which must control the error of individual low rank approximations of off-diagonal blocks.

With that said, there are of course circumstances in which the cost of using this log-likelihood evaluation strategy is not worth the higher prefactor than, say, the debiased Whittle approximation [29]. If one has a dataset with 50 000 measurements that needs to be fitted once, for example, it is probably worth spending an entire two to three minutes to obtain an effectively exact MLE instead of the 15 seconds it might take to obtain an approximate estimator from, say, the debiased Whittle method. Or at the least, it is likely worth refining that more computationally expedient estimator using the more accurate methods introduced here. But for an online application, on the other hand, or a setting in which one must fit tens or hundreds of datasets, a much cheaper method that runs in seconds instead of minutes may be worth the additional variance of the estimator.

Acknowledgements

The author is grateful to Paul G. Beckman for his thoughtful comments, discussion, and proofreading of the manuscript.

References

- [1] S. Ambikasaran, M. O’Neil, and K.R. Singh. Fast symmetric factorization of hierarchical matrices with applications. *arXiv preprint arXiv:1405.0223*, 2014.
- [2] S. Ambikasaran, D. Foreman-Mackey, L. Greengard, D.W. Hogg, and M. O’Neil. Fast direct methods for gaussian processes. *IEEE transactions on pattern analysis and machine intelligence*, 38(2):252–265, 2015.
- [3] M. Anitescu, J. Chen, and L. Wang. A matrix-free approach for solving the parametric gaussian process maximum likelihood problem. *SIAM Journal on Scientific Computing*, 34(1):A240–A262, 2012.
- [4] H. Avron and S. Toledo. Randomized algorithms for estimating the trace of an implicit symmetric positive semi-definite matrix. *Journal of the ACM (JACM)*, 58(2):1–34, 2011.
- [5] A.H. Barnett, J. Magland, and L. af Klinteberg. A parallel nonuniform fast Fourier transform library based on an “exponential of semicircle” kernel. *SIAM Journal on Scientific Computing*, 41(5):C479–C504, 2019.
- [6] Paul G Beckman and Christopher J Geoga. Fast adaptive fourier integration for spectral densities of gaussian processes. *arXiv preprint arXiv:2404.19053*, 2024.
- [7] J. Bezanson, A. Edelman, S. Karpinski, and V.B. Shah. Julia: A fresh approach to numerical computing. *SIAM review*, 59(1):65–98, 2017.
- [8] S. Börm, L. Grasedyck, and W. Hackbusch. Introduction to hierarchical matrices with applications. *Engineering analysis with boundary elements*, 27(5):405–422, 2003.
- [9] P.J. Brockwell and R.A. Davis. *Time series: theory and methods*. Springer science & business media, 1991.
- [10] J. Chen and M.L. Stein. Linear-cost covariance functions for gaussian random fields. *Journal of the American Statistical Association*, 118(541):147–164, 2023.

- [11] A. Deaño, D. Huybrechs, and A. Iserles. *Computing highly oscillatory integrals*. SIAM, 2017.
- [12] A. Dutt and V. Rokhlin. Fast Fourier transforms for nonequispaced data. *SIAM Journal on Scientific computing*, 14(6):1368–1393, 1993.
- [13] Bradley Efron and David V Hinkley. Assessing the accuracy of the maximum likelihood estimator: Observed versus expected fisher information. *Biometrika*, 65(3):457–483, 1978.
- [14] D. Foreman-Mackey, E. Agol, S. Ambikasaran, and R. Angus. Fast and scalable gaussian process modeling with applications to astronomical time series. *The Astronomical Journal*, 154(6):220, 2017.
- [15] C.J. Geoga, M. Anitescu, and M.L. Stein. Scalable gaussian process computations using hierarchical matrices. *Journal of Computational and Graphical Statistics*, 29(2):227–237, 2020.
- [16] P. Gonnet. A review of error estimation in adaptive quadrature. *ACM Computing Surveys (CSUR)*, 44(4):1–36, 2012.
- [17] R.M. Gray. Toeplitz and circulant matrices: A review. *Foundations and Trends[®] in Communications and Information Theory*, 2(3):155–239, 2006.
- [18] L. Greengard and V. Rokhlin. A fast algorithm for particle simulations. *Journal of computational physics*, 73(2):325–348, 1987.
- [19] L. Greengard and J. Strain. The fast gauss transform. *SIAM Journal on Scientific and Statistical Computing*, 12(1):79–94, 1991.
- [20] L. Greengard, J.Y. Lee, and S. Inati. The fast sinc transform and image reconstruction from nonuniform samples in k-space. *Communications in Applied Mathematics and Computational Science*, 1(1):121–131, 2007.
- [21] N. Halko, P.G. Martinsson, and J.A. Tropp. Finding structure with randomness: Probabilistic algorithms for constructing approximate matrix decompositions. *SIAM review*, 53(2):217–288, 2011.
- [22] C.C. Heyde. *Quasi-likelihood and its application: a general approach to optimal parameter estimation*. Springer, 1997.
- [23] S.G. Johnson. QuadGK.jl: Gauss–Kronrod integration in Julia. <https://github.com/JuliaMath/QuadGK.jl>, 2013.
- [24] A. Litvinenko, Y. Sun, M.G. Genton, and D.E. Keyes. Likelihood approximation with hierarchical matrices for large spatial datasets. *Computational Statistics & Data Analysis*, 137:115–132, 2019.
- [25] V. Minden, A. Damle, K.L. Ho, and L. Ying. Fast spatial gaussian process maximum likelihood estimation via skeletonization factorizations. *Multiscale Modeling & Simulation*, 15(4):1584–1611, 2017.
- [26] M.L. Stein. Limitations on low rank approximations for covariance matrices of spatial data. *Spatial Statistics*, 8:1–19, 2014.
- [27] M.L. Stein, J. Chen, and M. Anitescu. Stochastic approximation of score functions for gaussian processes. *The Annals of Applied Statistics*, pages 1162–1191, 2013.
- [28] S. Subba Rao and J. Yang. Reconciling the gaussian and whittle likelihood with an application to estimation in the frequency domain. *The Annals of Statistics*, 49(5):2774–2802, 2021.
- [29] A.M. Sykulski, S.C. Olhede, A.P. Guillaumin, J.M. Lilly, and J.J. Early. The debiased whittle likelihood. *Biometrika*, 106(2):251–266, 2019.
- [30] L.N. Trefethen. *Approximation theory and approximation practice, extended edition*. SIAM, 2019.
- [31] J.A. Tropp and R.J. Webber. Randomized algorithms for low-rank matrix approximation: Design, analysis, and applications. *arXiv preprint arXiv:2306.12418*, 2023.

- [32] P. Whittle. Estimation and information in stationary time series. *Arkiv för matematik*, 2(5):423–434, 1953.
- [33] A.T.A. Wood and G. Chan. Simulation of stationary gaussian processes in $[0, 1]$ d. *Journal of computational and graphical statistics*, 3(4):409–432, 1994.